Nano Energy 66 (2019) 104149

Contents lists available at ScienceDirect

Nano Energy

journal homepage: http://www.elsevier.com/locate/nanoen

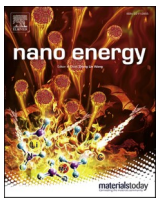

Communication

A wearable system based on core-shell structured peptide-Co_9S_8 supercapacitor and triboelectric nanogenerator

Wei Xiong [a,b,1], Kuan Hu [b,c,1], Zhe Li [b,1], Yixiang Jiang [c], Zigang Li [c,d,**], Zhou Li [b,*], Xinwei Wang [a,***]

[a] School of Advanced Materials, Shenzhen Graduate School, Peking University, Shenzhen, 518055, China
[b] Beijing Institute of Nanoenergy and Nanosystems, Chinese Academy of Sciences, Beijing, 100083, China
[c] Key Laboratory of Chemical Genomics, School of Chemical Biology and Biotechnology, Shenzhen Graduate School, Peking University, Shenzhen, 518055, China
[d] Pingshan Translational Medicine Center, Shenzhen Bay Laboratory, Shenzhen, 518055, China

ARTICLE INFO

Keywords:
Peptide
Co_9S_8
ALD
Supercapacitor
TENG

ABSTRACT

We report a new core-shell structure of peptide-Co_9S_8 nanobricks for supercapacitor electrode. The nanostructured peptide is intrinsically flexible and biocompatible, which is highly suited for wearable supercapacitor electrodes. However, the application of the nanostructured peptide is often limited by its generally low power density and energy density, and its long-term stability is also a concern. Herein, the core-shell structure of peptide-Co_9S_8 nanobricks is synthesized by conformally coating a thin shell layer of Co_9S_8 via atomic layer deposition (ALD) onto self-assembled peptide nanobricks. The shell layer can not only protect the peptide material from being attacked by the electrolyte but also contribute extra capacitance to the supercapacitor. The supercapacitors made of the peptide-Co_9S_8 nanobricks exhibit a high capacitance of 1.3 F/cm^2 at 0.7 mA/cm^2 and a much improved cycling stability of 96% capacitance retention after 5000 charge-discharge cycling. High-performance flexible solid-state asymmetric supercapacitor (SC) can be also made from the core-shell peptide-Co_9S_8 nanobricks with activated carbon. The flexible asymmetric supercapacitor can also be coupled with a triboelectric nanogenerator (TENG) to afford a flexible self-powered TENG/SC system. The TENG/SC system with 2.7-h continuously charging by TENG can power a red LED for 21 min, which demonstrates its excellent performance of self-charging and energy-supplying, and therefore it is of great promise for future wearable electronics applications.

1. Introduction

Wearable technology is regarded as a very important sector in the modern Internet of Things (IoT) [1–4], and significant research effort has been devoted to the development of high-performance wearable power sources. Electrochemical supercapacitor is regarded as a highly important wearable power source technology, and it is renowned for excellent charge–discharge cycling stability and able to deliver a high power of electricity [5–11].Although the energy density of supercapacitors is generally lower than batteries, this issue could be remedied by coupling a supercapacitor with an electricity generator (both wearable), such as a triboelectric nanogenerator (TENG), which can convert mechanical motion energy into electricity [12–15], thereby intermittently powering the supercapacitor. Together, this wearable power source technology is highly suited for many contemporary motion monitoring circuits.

As for the supercapacitor materials, the electrochemically active materials on the electrodes are of the crucial importance to achieve high power density, good stability, and flexibility for the wearable supercapacitors. Traditionally, many carbon-based materials, such as carbon nanotubes (CNTs), graphene derivatives, and activated carbon were assessed in this regard, but the specific capacitance obtained from the

* Corresponding author.
** Corresponding author. State Key Laboratory of Chemical Oncogenomics, School of Chemical Biology and Biotechnology, Shenzhen Graduate School of Peking University, Shenzhen, 518055, China.
*** Corresponding author.
E-mail addresses: lizg@pkusz.edu.cn (Z. Li), zli@binn.cas.cn (Z. Li), wangxw@pkusz.edu.cn (X. Wang).
[1] These authors contributed equally to this work.

https://doi.org/10.1016/j.nanoen.2019.104149
Received 29 August 2019; Received in revised form 17 September 2019; Accepted 28 September 2019
Available online 2 October 2019

carbon materials is much lower than expected, mainly due to the poor wettability of the carbon materials [16–20]. Recently, nanostructured biomaterials, such as peptides, have emerged as new promising candidate materials for supercapacitors [16,21,22]. Molecularly engineered peptide molecules could self-assemble into certain nanostructures (e.g. nanotubes [16,22], nanofibers [23], and nanosheets [24,25]), which have exhibited promising supercapacitor performance. Compared to traditional materials, the peptide-based bio-nanomaterials are of the merits being readily available, cost effective, intrinsically flexible, and structurally stable and versatile, and in particular, the flexible while stable three-dimensional molecular framework is ideally suited to provide the flexibility and reliability for wearable energy storage. In addition, the peptide materials are naturally of good biocompatibility, and therefore they are also potentially suitable for implanted devices applications.

Despite a number of advantages along with numerous promising reports [26–28], the performance of the supercapacitors based on peptide nanomaterials is still far lagged behind the inorganic counterparts in general. Both the power density and energy density of the peptide supercapacitors are comparatively low; and their long-term cycling stability is also a concern, especially in an acidic or alkaline electrolyte, owing to the catalyzed hydrolysis of the amide bonds in peptides. To enhance the performance of the peptide supercapacitors, we herein propose to adopt a novel technology of atomic layer deposition (ALD) to coat the peptide nanostructure with a uniform conformal layer of Co_9S_8 to afford a peptide-Co_9S_8 core-shell nanostructure. ALD is renowned for coating a conformal layer with highly controlled thickness while not to alter the morphology of the underneath substrate structure [29–32]. By elaborately manipulating the thickness of ALD Co_9S_8 shell, optimized Co_9S_8 shell could be screened out. The Co_9S_8 coating layer provides dual functionalities, as it can not only protect the inside peptides from being chemically attacked by the electrolyte, but the Co_9S_8 material itself is electrochemically active and therefore can additionally boost the overall capacitance of the supercapacitors. With the implementation of this idea, we show in the following that the synthesized core-shell peptide-Co_9S_8 nanobricks are able to withstand harsh alkaline conditions, and therefore the supercapacitors made of the peptide-Co_9S_8 nanobricks exhibit excellent stability for long-term charge–discharge cycling. We further show that high-performance flexible solid-state asymmetric supercapacitor can be made from the core-shell peptide-Co_9S_8 nanobricks with activated carbon, and the asymmetric supercapacitor can also be coupled with a triboelectric nanogenerator (TENG) to afford a flexible self-powered system which is of great promise for future wearable electronics applications.

2. Results and discussion

A cyclic pentapeptide of Ac-CAAAS$_5$ (phenyl) (Scheme 1) was employed as the structural motif to be self-assembled into nanostructures. This type of peptide contains an in-tether chiral center, which was considered to be beneficial to afford a highly ordered molecule network thereby facilitating the self-assembling process [21]. With the in-tether phenyl substitution in the peptide, structures of nanobricks were formed by a self-assembling process. The material properties of the afforded peptide nanobricks were carefully characterized as the following. FTIR was employed to identify the chemical bonds and secondary structure of the assembly [33]. The FTIR spectrum (Fig. 1a) displays an intense band for amide I at 1654 cm^{-1} and two intense bands for amide II at 1530 and 1547 cm^{-1}, which indicates an α-helical structure [34]. This indication is also corroborated by the presence of a weak amide III band at 1308 cm^{-1}. Also, two N-H stretching bands were found at 3319 and 3266 cm^{-1} (Fig. 1a inset), which suggests the presence of a hydrogen bond network and also implies a helical structure for each individual peptide molecule. XRD was used to examine the crystallinity of the peptide nanobricks. The XRD pattern (Fig. 1b) shows a set of diffraction peaks at 3.6, 5.2, 10.5, 15.7, 26.3, and 31.7°, which indicates that the self-assembled peptide nanobricks were crystalline. The crystalline nature of the self-assembly was desirable, as it suggests a good chemical and thermal stability of the peptide nanostructure. The morphology of the peptide nanobricks was examined by SEM (Fig. 1c), and the size of the nanobricks was found to be about ~10 μm in length and 3–4 μm in width.

We then investigated the electrochemical supercapacitor behavior of the peptide nanobricks. The peptide nanobricks were loaded onto a glassy carbon (GC) electrode for cyclic voltammetry (CV) measurement, which was carried out with a three-electrode configuration in 1 M KOH. For comparison purposes, home-made polypyrrole (PPy) and polyaniline (PANI) nanowires as well as commercial CNTs (Fig. S1) were used as the benchmarking active materials, because these materials were often used for supercapacitors [5,7,12,35]. Fig. 2a shows the CV results with a voltage scan rate of 20 mV/s for a potential range from 0 to 1 V (versus Hg/HgO). All the CV curves are nearly rectangular-shaped, which suggests that the capacitances were mostly contributed from the electrical double-layer capacitances (EDLCs). Note that the bare GC electrode had negligible capacitance contribution. Clearly, the integral area of the CV curve was significantly larger for the peptide nanobricks than those for the PPy and PANI nanowires, and it was only slightly smaller than that for the CNTs. These results indicate that the peptide nanobricks themselves had a high specific capacitance (Fig. S2i), owing to their high specific surface area. Electrochemical impedance spectroscopy (EIS) measurement (Fig. S2j) further showed that the peptide nanobricks electrode had a quite small series resistance (R_s) of 7.4 Ω, which was appreciably smaller than those of PPy (10.0 Ω) and PANI nanowires (10.8 Ω) and comparable to that of CNTs (6.4 Ω). The small series resistance was due to a better hydrophilicity of the peptide than that of PPy or PANI, which could lower the contact resistance at the interface between the electrode and electrolyte [36,37].

Apparently, all the above electrochemical characterizations suggested that the self-assembled peptide nanobricks were a promising candidate material for supercapacitors. However, unfortunately, the long-term stability of the peptide nanobricks was not sufficiently good. As shown in Fig. 2d, the capacitance retention was only 67% of its initial

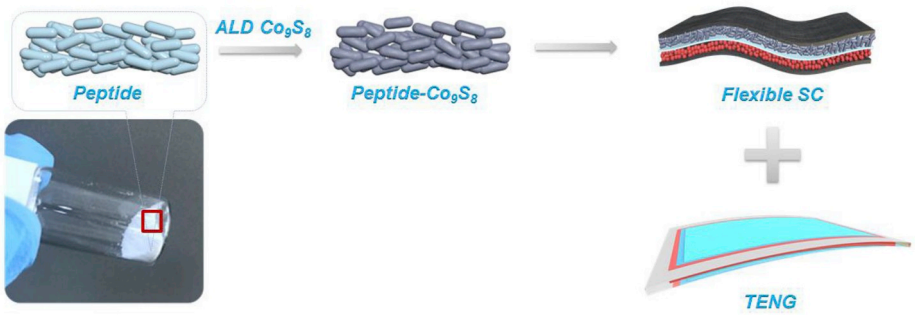

Scheme 1. Preparation for peptide-Co_9S_8 core-shell nanostructures and TENG/SC system.

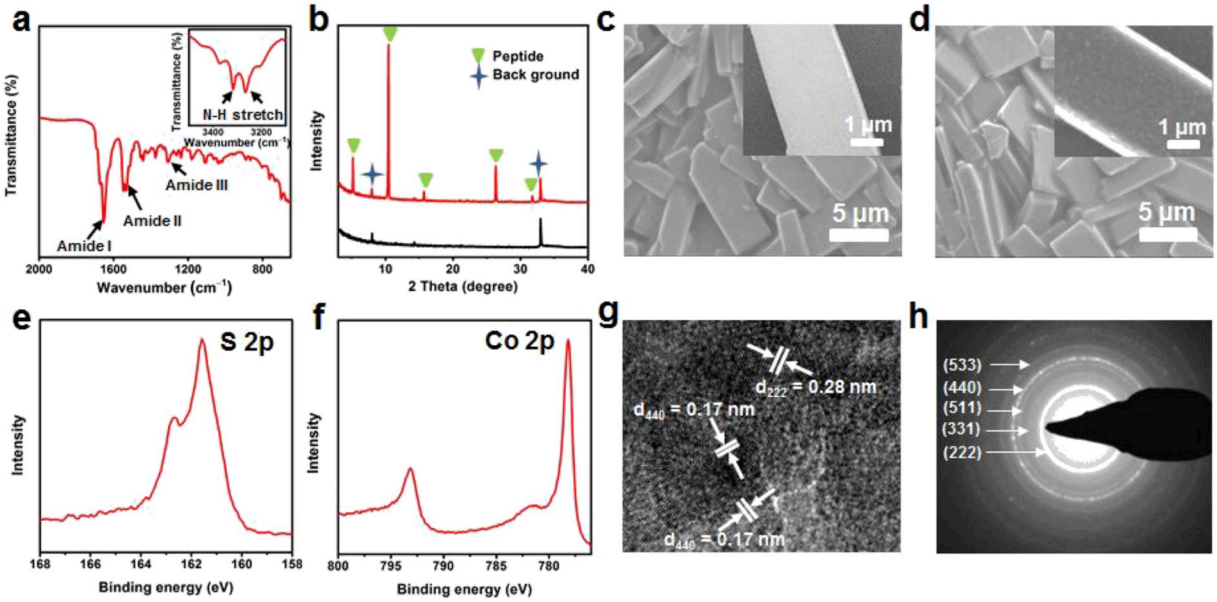

Fig. 1. (a) FTIR spectrum and (b) XRD spectrum of self-assembled peptide nanobricks. SEM images of the peptide nanobricks (c) before and (d) after the ALD of 50 nm Co_9S_8. (e, f) High-resolution S 2p and Co 2p XPS spectra. (g) HRTEM image and (h) the corresponding electron diffraction pattern of the peptide-Co_9S_8, showing the presence of the Co_9S_8 shell.

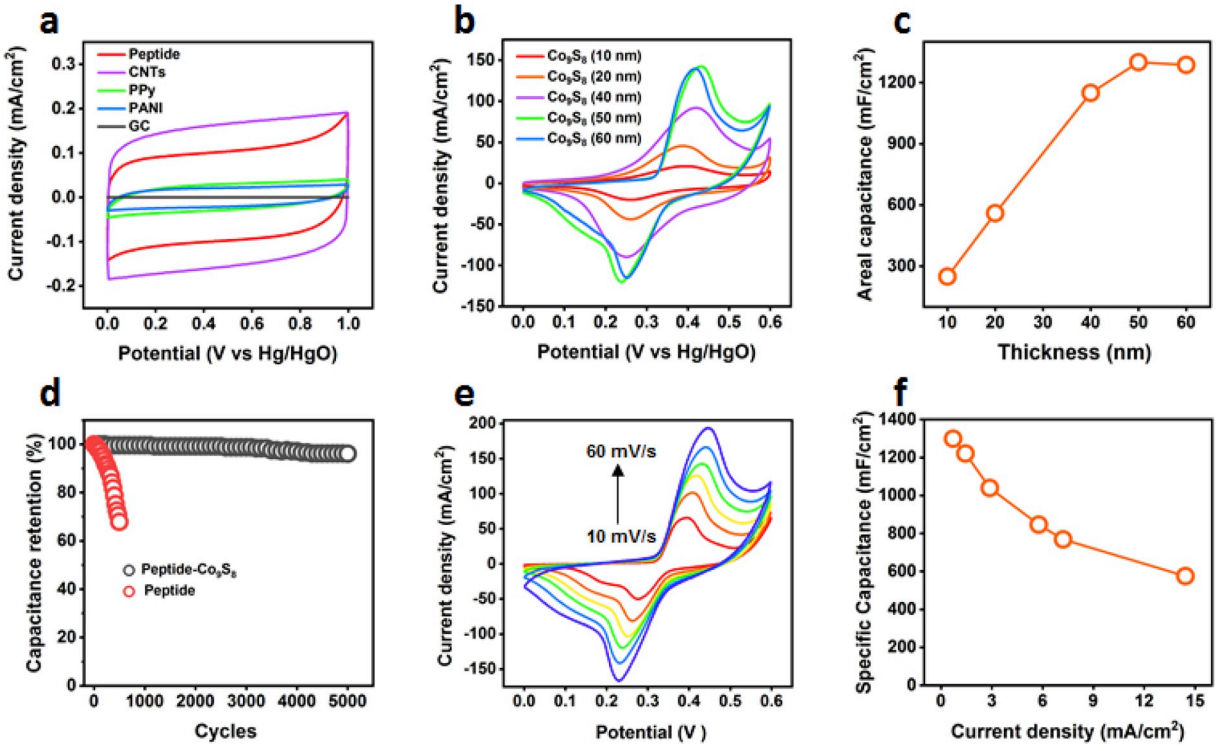

Fig. 2. (a) CV curves for the peptide nanobricks, CNTs, PPy nanowires, PANI nanowires, and bare GC. The scan rate was 20 mV/s (b) CV curves for the peptide-Co_9S_8 with various Co_9S_8 shell thicknesses and (c) the corresponding plot of the areal capacitance versus Co_9S_8 thickness. The scan rate was 40 mV/s. (d) Cycling performances of the peptide-Co_9S_8 and peptide electrodes at current density of 0.1 mA/cm^2 (e) CV curves of the peptide-Co_9S_8 at various scan rates ranging from 10 to 60 mV/s. (f) Plot of the specific capacitance of the peptide-Co_9S_8 versus the current density.

value after 500 charge–discharge cycles. The degradation was due to the hydrolysis of the peptide amide bonds in alkaline, which could dissemble the structure of the peptide nanobricks. Indeed, as shown in Fig. S3a, the well-ordered peptide nanobricks became slurry-like after the charge–discharge cycling. To overcome the stability issue, we adopted an ALD approach to coat a thin protective layer of Co_9S_8 on the peptide nanobricks. Notably, Co_9S_8 itself has a good redox performance [32], and therefore the Co_9S_8 coating layer can also provide additional contribution to the capacitance. ALD is renowned for coating a conformal layer without altering the topology of the underneath substrate structure and indeed the post-ALD Co_9S_8-coated peptide assembly well retained the original nanobrick morphology. As shown in Fig. 1d, a

representative post-ALD sample with 50 nm Co_9S_8 on the peptide nanobricks exhibits almost the same morphology as compared to that before ALD. The presence of the Co_9S_8 layer was confirmed by XPS. As shown in Fig. 1e and f, the high-resolution XPS S 2p spectrum shows a pair of spin-orbit split peaks at the binding energies of 161.4 and 162.5 eV, and the Co 2p spectrum shows a pair of spin-orbit split peaks at the binding energies of 778.3 and 793.2 eV, which all agree with the reported data for Co_9S_8 [32,38]. High-resolution TEM image (Fig. 1g) shows clear lattice fringes which correspond to the face-centered cubic (fcc) structure of Co_9S_8 (JCPDS 86–2273). The associated electron diffraction pattern (Fig. 1h) displays clear diffraction rings, which also agree with the fcc Co_9S_8 structure.

The electrochemical properties of the ALD peptide-Co_9S_8 was then investigated. We first investigated the effect of the Co_9S_8 coating thickness. Fig. 2b shows the CV curves of the peptide-Co_9S_8 with the Co_9S_8 layer thickness ranging from 10 to 60 nm. Unlike the uncoated peptide nanobricks, the CV curves of the peptide-Co_9S_8 composites exhibited pronounced redox peaks, which increased in magnitude with the increase of the Co_9S_8 layer thickness up to 50 nm, suggesting that there was additional Faradaic pseudocapacitance contribution from the redox reaction of Co_9S_8 in alkaline [32]. In particular, the capacitance of the 10 nm Co_9S_8-coated peptide-Co_9S_8 composite was ~50 times more than that of the uncoated peptide nanobricks. Fig. 2c plots the capacitance with respect to the Co_9S_8 layer thickness, which shows that the areal capacitance increased when the thickness increased from 10 to 50 nm and saturated when the thickness exceeded 50 nm. This saturation was due to the diffusion limit of proton in the Co_9S_8 layer, as proton was considered participating in the redox reaction of Co_9S_8 [5,39]. Therefore, unless otherwise specified, the optimal Co_9S_8 layer thickness of 50 nm was chosen for the following experiments. The charge−discharge cycling performance was significantly enhanced by the ALD Co_9S_8 layer. As shown in Fig. 2d, the peptide-Co_9S_8 composite with a 50 nm Co_9S_8 layer was able to retain 96% of its initial capacitance after 5000 charge−discharge cycles. Also, the nanobrick architecture was well preserved after the cycling, as shown in Fig. S3b. Therefore, we concluded that the ALD Co_9S_8 shell could effectively protect the peptide nanobricks upon electrochemical cycling.

In addition, we also carried out the CV measurement with various scan rates for the peptide-Co_9S_8. As shown in Fig. 2e, with the increase of scan rate from 10 to 60 mV/s, the current density increased in magnitude, but the general shape of the CV curves remained mostly the same, which is indicative of a fast redox reaction, therefore suggesting a good

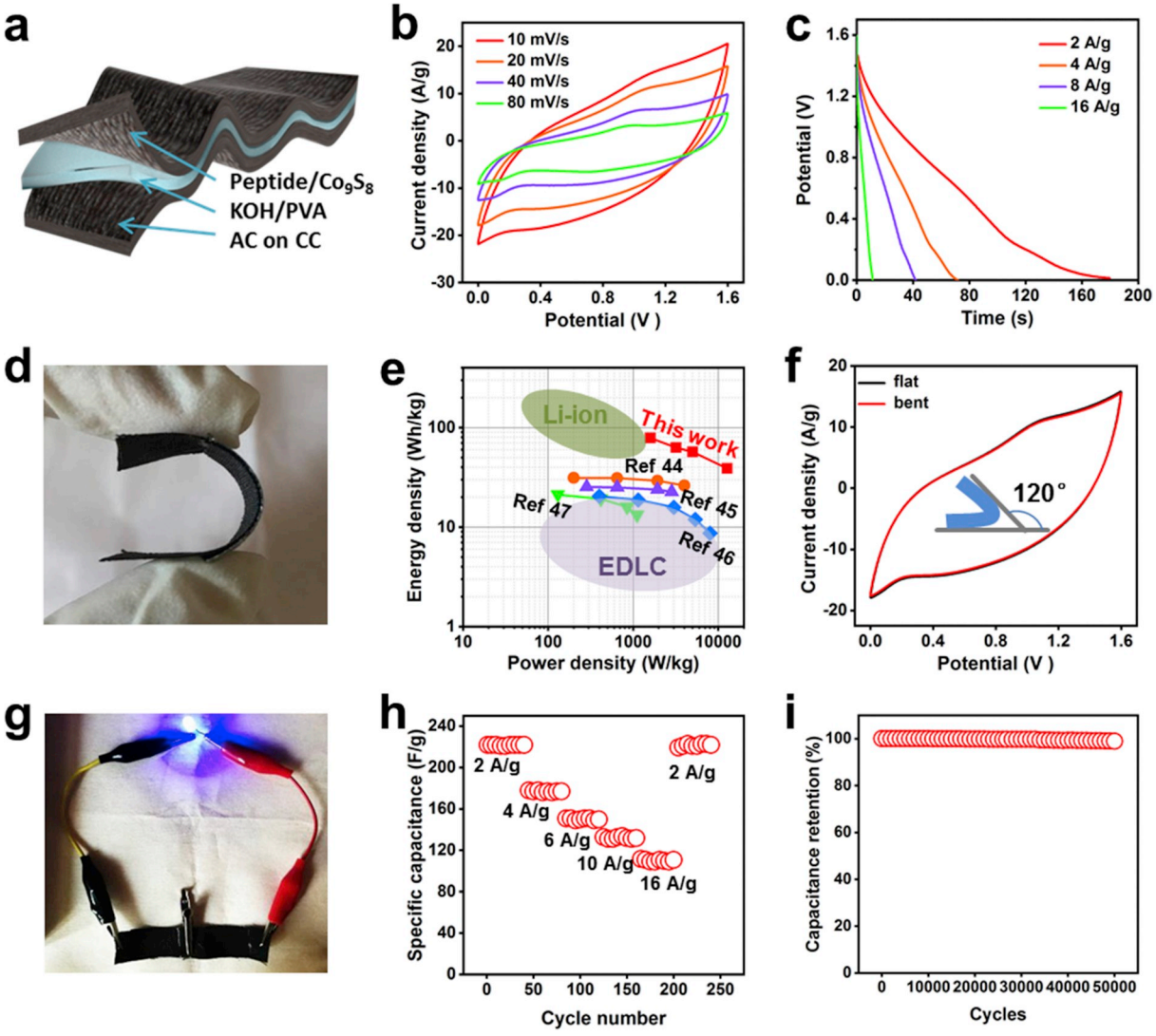

Fig. 3. (a) Schematic illustration of the peptide-Co_9S_8//AC flexible solid-state asymmetric supercapacitor. (b) CV curves of the peptide-Co_9S_8//AC supercapacitor with various scan rates. (c) Discharge curves at various current densities. (d) Photograph showing the flexibility of the supercapacitor device. (e) The Ragone plot. (f) CV curves comparing the flat-state and bent-state of the supercapacitor device (the bending angle was 120°). (g) Photograph showing an LED is lit by using two peptide-Co_9S_8//AC supercapacitors in series. (h) Cycling performance at various current densities. (i) Long-term cycling performance at current density of 16 A/g.

supercapacitor behavior at high charge−discharge rate. Fig. 2f shows the measured rate performance of the peptide-Co_9S_8, where the specific capacitance was obtained by galvanostatic discharging (Fig. S4) and is plotted with respect to current density. The peptide-Co_9S_8 exhibited a fairly high specific capacitance of 1300 mF/cm^2 (1800 F/g) at 0.7 mA/cm^2 with an outstanding capacitance retention of 44.5% (i.e. 578.5 mF/cm^2) at 14 mA/cm^2. Such a high specific capacitance and a good rate performance outperformed many other core-shell nanostructured materials, such as TiO_2@NiO nanotube array (2.9 mF/cm^2 at 0.4 mA/cm^2) [40], Fe_2O_3@PANI nanowires (103 mF/cm^2 at 0.9 mA/cm^2) [41], PEDOT@MnO_2 nanowires (426 mF/cm^2 at 10 mA/cm^2) [42], and V_2O_5@PPy network (112 mF/cm^2 at 0.1 mA/cm^2) [43].

To further demonstrate the practical application of the peptide-Co_9S_8 composite, a flexible solid-state asymmetric supercapacitor (namely peptide-Co_9S_8//AC) was assembled (Fig. 3a), using the peptide-Co_9S_8 composite and activated carbon (AC) as the cathode and anode materials, respectively. The CV curves of the supercapacitor device were measured in the voltage range of 0–1.6 V with various scan rates. As shown in Fig. 3b, the shape of the CV curves is in accordance with the features combining from the double-layer capacitive contribution from AC and the pseudocapacitance contribution from the peptide-Co_9S_8 [37]. Fig. 3c shows the galvanostatic discharging curves at various current densities from 2 to 16 A/g (see also Fig. S5). Accordingly, Fig. 3e shows the gravimetric power and energy densities of our device. Notably, these densities were calculated based on the total mass of the device, including the masses of the electrolyte and electrodes. Two circles shown in the plot represent the ranges for typical lithium-ion batteries (LIBs) and EDLCs. Clearly, the peptide-Co_9S_8//AC supercapacitor device was able to deliver a very high energy density of 79 Wh/kg at a power density of 1.6 kW/kg, which is even comparable to typical LIBs; and the device was also able to deliver a very high power density of 12.8 kW/kg at an energy density of 39 Wh/kg, which is significantly better than the numbers for typical EDLCs. Compared to other reported solid-state supercapacitors [44–47], the gravimetric energy and power densities obtained herein are also fairly high, which highlights the superior advantages of using the peptide-Co_9S_8 core-shell nanobricks for supercapacitors. Fig. S6a also compares the corresponding volumetric power and energy densities. The maximum volumetric energy density of our device was 3.0 mWh/cm^3, which is also much better than many solid-state energy storage devices [48–51], even reaching the level of thin-film lithium battery (0.3–10 mWh/cm^3) [52]. In addition, the leakage current of our device was found to be fairly low as 9.1 μA (Fig. S6b). The fabricated supercapacitors were also highly flexible (Fig. 3d), and they could be bent to a large angle of 120° without changing its performance (Fig. 3f). The cycling performance was also good. As shown in Fig. 3h, upon continuous charge−discharge cycling sequentially at different current densities from 2 to 16 A/g, no appreciable capacitance decay was observed when the current density was switched back to its initial value. Therefore, the peptide-Co_9S_8//AC device was quite stable upon the charging and discharging at high rate. The long-term cycling performance was also evaluated by continuously charging and discharging at a galvanostatics. current density of 16 A/g. As shown in Fig. 3i, 98% of the initial capacitance was retained even after 50000 cycles. These results clearly demonstrate the excellent long-term cycling stability of the peptide-Co_9S_8//AC supercapacitor. Fig. 3g also shows a practical use of two peptide-Co_9S_8//AC supercapacitors in series to lighten a commercial light-emitting diode, which requires a driving potential of ~3.0 V.

To further explore the applications of the peptide-Co_9S_8//AC supercapacitor for wearable devices, we designed a self-powered system by integrating a flexible peptide-Co_9S_8//AC supercapacitor with a triboelectric nanogenerator (TENG), namely the TENG/SC system. Using the high-performance supercapacitor to temporarily store the electrical energy intermittently generated by a TENG device, the integrated TENG/SC system could provide significantly better performance than the TENG itself to power wearable electronic devices. A TENG device couples the triboelectrification and electrostatic induction, and it is a powerful technique to convert the omnipresent mechanical energy into electricity [5,12,13,53–55]. TENG also has numerous advantages such as low cost, high and stable energy-conversion efficiency, and good shape-adaptability [12,14]. To date, wearable and implantable TENGs have been shown with tremendous potential and advantages as wearable power sources [12,15,56–59]. In this work, a flexible light-weight encapsulated TENG (Fig. 4a) was used to harvest the energy from mechanical pressing. The detailed working principle of coupling the contact electrification and electrostatic induction for TENG is illustrated in Fig. S7. Upon contacting and releasing, electrons were driven back and forth through the external circuit to generate electricity. As shown in Fig. 4b and c, a piece of 2.0 × 3.0 cm^2 TENG (Fig. S8) can output a very high peak voltage of 9.0 V with a peak current of 8.2 μA. The enlarged waveshapes of the voltage and current are shown in Figs. S9a and b. The TENG was also quite flexible (Fig. 4e) and stable, as no apparent change in the output voltage was observed for 17.5-h continuously contacting and releasing (Fig. 4d). The excellent flexibility and stability of TENG is highly desirable for the integration with the peptide-Co_9S_8//AC supercapacitor. The integrated TENG/SC system is shown in Fig. 4g, and the circuit diagram is shown in Fig. 4f. Fig. 4h shows that with 2.7-h continuously charging by TENG, the peptide-Co_9S_8//AC supercapacitor can power a red LED for 21 min, demonstrating the high efficiency of the self-powering functionality of the integrated TENG/SC system. Notably, no appreciable self-discharging was observed for a long period of several hours. All these features have suggested that the TENG/SC system is highly suited for wearable devices. To further demonstrate an example of the TENG/SC system for a practical wearable device, the TENG/SC system was integrated into a watch band, which could sense the pulse signals at human wrist and convert the pulse signals into electricity. Note that the TENG device is able to sense the wrist pulse (Fig. 4i): the average output peak voltage and current were 2.9 mV and 0.2 mA, respectively (Fig. 4j and k). When a sufficient amount of energy was stored, the TENG/SC system was able to power a commercial watch (Fig. 4l). These results clearly demonstrate the great promise of the TENG/SC system for wearable electronics applications.

3. Conclusion

In summary, we reported a novel core-shell nanobrick structure of peptide-Co_9S_8, which is highly promising for wearable supercapacitor applications. The synthesized peptide-Co_9S_8 nanostructure was composed of self-assembled peptide nanobricks as the core and a thin conformal Co_9S_8 shell layer which was made by an advanced technology of ALD. With this protective Co_9S_8 shell layer, the peptide nanobricks were able to withstand in harsh alkaline electrolyte, and in addition, the Co_9S_8 layer could also provide extra contribution to the capacitance. With an optimal 50 nm Co_9S_8 shell, the peptide-Co_9S_8 core-shell nanobricks exhibited an excellent charge–discharge cycling performance for 96% capacitance retention over 5000 cycles, as compared to the uncoated peptide with only 67% capacitance retention for only 500 cycles; meanwhile, the specific capacitance of the peptide-Co_9S_8 achieved a fairly high value of 1300 mF/cm^2 (1800 F/g) at 0.7 mA/cm^2. These results clearly demonstrate the importance of the dual-functional ALD Co_9S_8 shell, which enables the core-shell nanostructured peptide-Co_9S_8 as a promising candidate material for supercapacitor applications. To further demonstrate its applications, the peptide-Co_9S_8 was coupled with AC to fabricate the high-performance solid-state asymmetric supercapacitor of peptide-Co_9S_8//AC. The fabricated peptide-Co_9S_8//AC supercapacitor was highly flexible, and it could deliver remarkably high energy density and power density. To further explore its applications for wearable devices, the flexible peptide-Co_9S_8//AC supercapacitor was integrated with a triboelectric nanogenerator (TENG) to afford a wearable self-powered TENG/SC system. The afforded TENG/SC system was demonstrated to show the excellent performance of self-charging and energy-supplying, and therefore it is of great promise for

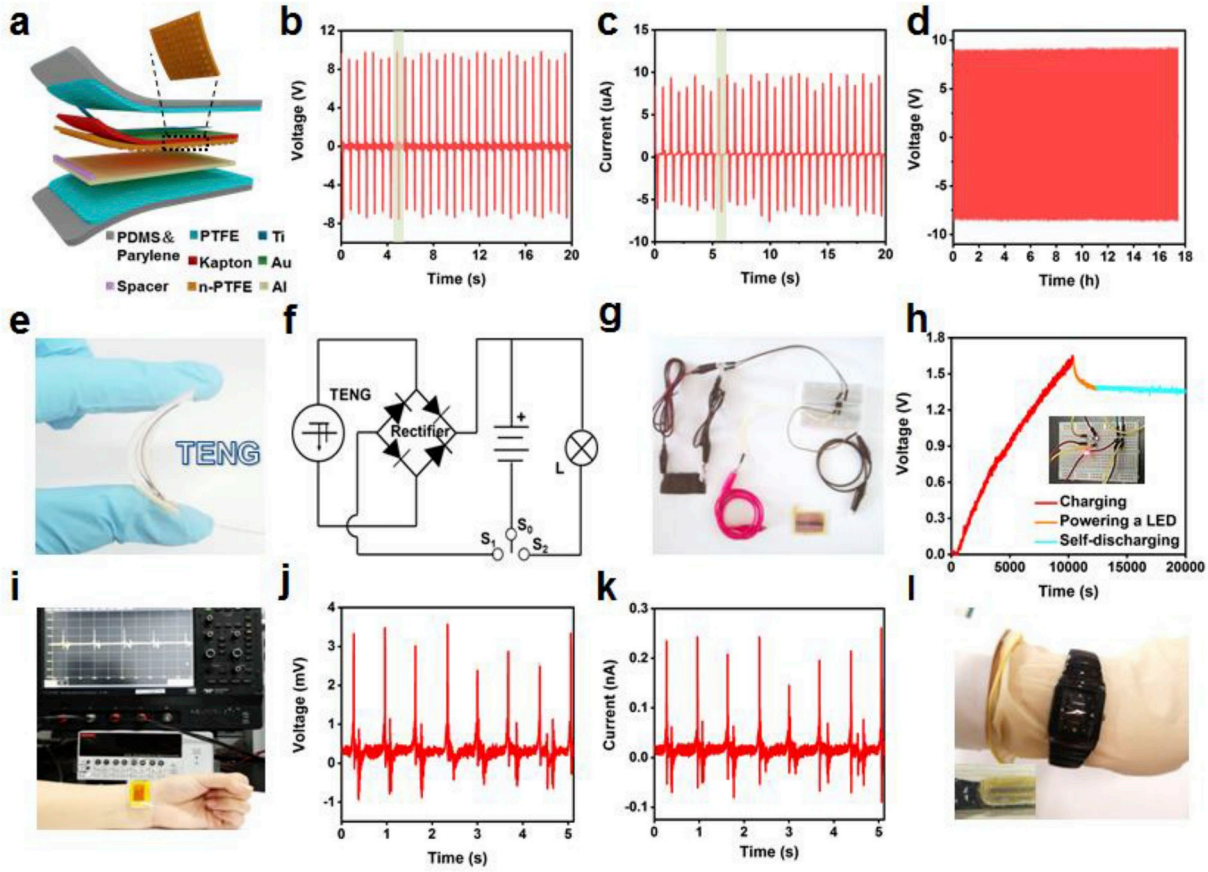

Fig. 4. (a) Schematic illustration of the structure of a TENG. (b) Output voltage and (c) current of a TENG upon contacting and releasing. (d) Trace of the output voltage for long-term continuous contacting and releasing. (e) Photograph of a bent TENG. (f) Circuit diagram and (g) photograph of the integrated TENG/SC system, containing TENG, SC, rectifier, and load. (h) The voltage curve showing the charging, working, and self-discharging stages. The inset photograph shows the TENG/SC system is powering a red LED. (i) Photograph showing a TENG is placed at the wrist to sense the pulse, and the associated (j) voltage and (k) current output traces. (l) Photograph showing a watch is powered by a TENG/SC system.

future wearable electronics applications.

Declaration of competing interest

The authors declare no conflict of interest.

Acknowledgments

This work was financially supported by NSFC (Grant No. 51672011, 51961165105, 61875015, 31571006, 21801019), Guangdong Natural Science Funds for Distinguished Young Scholar (Grant No. 2015A030306036), Shenzhen Science and Technology Innovation Committee (Grant No. JCYJ20180302150402760), and the National Youth Talent Support Program.

Appendix A. Supplementary data

Supplementary data to this article can be found online at https://doi.org/10.1016/j.nanoen.2019.104149.

References

[1] E.G. Jeong, Y. Jeon, S.H. Cho, K.C. Choi, Energy Environ. Sci. 12 (2019) 1878–1889.
[2] S. Kwon, H. Kim, S. Choi, E.G. Jeong, D. Kim, S. Lee, H.S. Lee, Y.C. Seo, K.C. Choi, Nano Lett. 18 (2018) 347–356.
[3] H. Jinno, K. Fukuda, X. Xu, S. Park, Y. Suzuki, M. Koizumi, T. Yokota, I. Osaka, K. Takimiya, T. Someya, Nat. Energy 2 (2017) 780–785.
[4] S. Lee, Y. Lee, J. Park, D. Choi, Nano Energy 9 (2014) 88–93.
[5] X. Nan, C. Zhang, C. Liu, M. Liu, Z.L. Wang, G. Cao, ACS Appl. Mater. Interfaces 8 (2016) 862–870.
[6] M. Beidaghi, Y. Gogotsi, Energy Environ. Sci. 7 (2014) 867–884.
[7] Z.L. Li, X.S. Zhao, Chem. Soc. Rev. 38 (2009) 2520–2531.
[8] W. Xiong, Y. Gao, X. Wu, X. Hu, D. Lan, Y. Chen, X. Pu, Y. Zeng, J. Su, Z. Zhu, ACS Appl. Mater. Interfaces 6 (2014) 19416–19423.
[9] W. Xiong, X. Hu, X. Wu, Y. Zeng, B. Wang, G. He, Z. Zhu, J. Mater. Chem. A 3 (2015) 17209–17216.
[10] C. Wang, Y. Xi, M. Wang, C. Zhang, X. Wang, Q. Yang, W. Li, C. Hu, D. Zhang, Nano Energy 28 (2016) 115–123.
[11] P. Ji, J. Wan, Y. Xi, Y. Guan, C. Zhang, X. Gu, J. Li, J. Lu, D. Zhang, Nanotechnology 30 (2019) 335401.
[12] P. Liu, J. Yan, Z. Guang, Y. Huang, X. Li, W. Huang, J. Power Sources 424 (2019) 108–130.
[13] Z.L. Wang, T. Jiang, L. Xu, Nano Energy 39 (2017) 9–23.
[14] Z. Li, K. Hu, M. Yang, Y. Zou, J. Yang, M. Yu, H. Wang, X. Qu, P. Tan, C. Wang, X. Zhou, Z. Li, Nano Energy 58 (2019) 852–861.
[15] Q. Tang, M.-H. Yeh, G. Liu, S. Li, J. Chen, Y. Bai, L. Feng, M. Lai, K.-C. Ho, H. Guo, C. Hu, Nano Energy 47 (2018) 74–80.
[16] P. Beker, I. Koren, N. Amdursky, E. Gazit, G. Rosenman, J. Mater. Sci. 45 (2010) 6374–6378.
[17] P. Beker, G. Rosenman, J. Mater. Res. 25 (2011) 1661–1666.
[18] P. Simon, Y. Gogotsi, Nat. Mater. 7 (2008) 845.
[19] P. Simon, A.F. Burke, Electrochem. Soc. Interface 17 (2008) 38–43.
[20] A.G. Pandolfo, A.F. Hollenkamp, J. Power Sources 157 (2006) 11–27.
[21] K. Hu, Y. Jiang, W. Xiong, H. Li, P.Y. Zhang, F. Yin, Q. Zhang, H. Geng, F. Jiang, Z. Li, Sci. Adv. 4 (2018) eaar5907.
[22] A.A. Lihi, A. Daniel, B. Peter, Y. Maya, S. Shiri, B. Ludmila, R. Gil, G. Ehud, Nat. Nanotechnol. 4 (2009) 849–854.
[23] C.A.E. Hauser, Z. Shuguang, Chem. Soc. Rev. 39 (2010) 2780–2790.
[24] K. Li, Z. Zhang, D. Li, W. Zhang, X. Yu, L. Wei, C. Gong, W. Gang, Z. Su, Adv. Funct. Mater. 29 (2018) 1801056.
[25] Y. Lin, M.R. Thomas, A. Gelmi, V. Leonardo, E.T. Pashuck, S.A. Maynard, Y. Wang, M.M. Stevens, J. Am. Chem. Soc. 139 (2017) 13592–13595.
[26] C. Gong, S. Sun, Y. Zhang, L. Sun, G. Wei, Nanoscale 11 (2019) 4147–4182.
[27] J. Zhang, X. Wu, Z. Gan, X. Zhu, Y. Jin, Nano Res 7 (2014) 929–937.

[28] G. Colherinhas, T. Malaspina, E.E. Fileti, ACS Omega 3 (2018) 13869–13875.
[29] W. Xiong, Q. Guo, Z. Guo, H. Li, R. Zhao, Q. Chen, Z. Liu, X. Wang, J. Mater. Chem. A 6 (2018) 4297–4304.
[30] W. Xiong, Z. Guo, H. Li, R. Zhao, X. Wang, ACS Energy Lett 2 (2017) 2778–2785.
[31] H. Li, Y. Shao, Y. Su, Y. Gao, X. Wang, Chem. Mater. 28 (2016) 1155–1164.
[32] H. Li, Y. Gao, Y. Shao, Y. Su, X. Wang, Nano Lett. 15 (2015) 6689–6695.
[33] D.A. Middleton, J. Madine, V. Castelletto, I.W. Hamley, Angew. Chem. Int. Ed. 52 (2013) 10537–10540.
[34] J.D. Hartgerink, J.R. Granja, R.A. Milligan, M.R. Ghadiri, J. Am. Chem. Soc. 118 (1996) 43–50.
[35] G.A. Snook, P. Kao, A.S. Best, J. Power Sources 196 (2011) 1–12.
[36] T. Lin, I.-W. Chen, F. Liu, C. Yang, H. Bi, F. Xu, F. Huang, Science 350 (2015) 1508–1513.
[37] C. Zhou, Y. Zhang, Y. Li, J. Liu, Nano Lett. 13 (2013) 2078–2085.
[38] J. Xu, Q. Wang, X. Wang, Q. Xiang, B. Liang, D. Chen, G. Shen, ACS Nano 7 (2013) 5453–5462.
[39] T. Brousse, D. Belanger, J.W. Long, J. Electrochem. Soc. 162 (2018) A5185–A5189.
[40] J.-H. Kim, K. Zhu, Y. Yan, C.L. Perkins, A.J. Frank, Nano Lett. 10 (2010) 4099–4104.
[41] X.-F. Lu, X.-Y. Chen, W. Zhou, Y.-X. Tong, G.-R. Li, ACS Appl. Mater. Interfaces 7 (2015) 14843–14850.
[42] X. Xia, D. Chao, Z. Fan, C. Guan, X. Cao, H. Zhang, H.J. Fan, Nano Lett. 14 (2014) 1651–1658.
[43] T. Qian, N. Xu, J. Zhou, T. Yang, X. Liu, X. Shen, J. Liang, C. Yan, J. Mater. Chem. A 3 (2015) 488–493.
[44] R.B. Rakhi, N.A. Alhebshi, D.H. Anjum, H.N. Alshareef, J. Mater. Chem. A 2 (2014) 16190–16198.
[45] S. Zhang, D. Li, S. Chen, X. Yang, X. Zhao, Q. Zhao, S. Komarneni, D. Yang, J. Mater. Chem. A 5 (2017) 12453–12461.
[46] X. Mao, Z. Wang, W. Kong, W. Wang, New J. Chem. 41 (2017) 1142–1148.
[47] T. Yao, Y. Li, D. Liu, Y. Gu, S. Qin, X. Guo, H. Guo, Y. Ding, Q. Liu, Q. Chen, J. Li, D. He, J. Power Sources 379 (2018) 167–173.
[48] R. Li, Y. Wang, C. Zhou, C. Wang, X. Ba, Y. Li, X. Huang, J. Liu, Adv. Funct. Mater. 25 (2015) 5384–5394.
[49] X. Lu, G. Wang, T. Zhai, M. Yu, S. Xie, Y. Ling, C. Liang, Y. Tong, Y. Li, Nano Lett. 12 (2012) 5376–5381.
[50] M.F. El-Kady, V. Strong, S. Dubin, R.B. Kaner, Science 335 (2012) 1326–1330.
[51] M. Kaempgen, C.K. Chan, J. Ma, Y. Cui, G. Gruner, Nano Lett. 9 (2009) 1872–1876.
[52] D. Pech, M. Brunet, H. Durou, P. Huang, V. Mochalin, Y. Gogotsi, P.-L. Taberna, P. Simon, Nat. Nanotechnol. 5 (2010) 651.
[53] F.-R. Fan, Z.-Q. Tian, Z. Lin Wang, Nano Energy 1 (2012) 328–334.
[54] B. Shi, Z. Li, Y. Fan, Adv. Mater. 30 (2018) 1801511.
[55] W. Jiang, H. Li, Z. Liu, Z. Li, J. Tian, B. Shi, Y. Zou, H. Ouyang, C. Zhao, L. Zhao, R. Sun, H. Zheng, Y. Fan, Z.L. Wang, Z. Li, Adv. Mater. 30 (2018) 1801895.
[56] H. Guo, X. Pu, J. Chen, Y. Meng, M.-H. Yeh, G. Liu, Q. Tang, B. Chen, D. Liu, S. Qi, C. Wu, C. Hu, J. Wang, Z.L. Wang, Sci.Rob. 3 (2018) eaat2516.
[57] X. Pu, L. Li, H. Song, C. Du, Z. Zhao, C. Jiang, G. Cao, W. Hu, Z.L. Wang, Adv. Mater. 27 (2015) 2472–2478.
[58] H. Ouyang, J. Tian, G. Sun, Y. Zou, Z. Liu, H. Li, L. Zhao, B. Shi, Y. Fan, Y. Fan, Adv. Mater. 29 (2017) 1703456.
[59] Q. Guan, G. Lin, Y. Gong, J. Wang, W. Tan, D. Bao, Y. Liu, Z. You, X. Sun, Z. Wen, Y. Pan, J. Mater. Chem. A 7 (2019) 13948–13955.

Wei Xiong received his B.S. degree from Shandong Normal University in 2013 and master degree from Central China Normal University in 2016. Currently, he is a Ph.D. candidate in the School of Advanced Materials, Peking University. His research focuses on atomic layer deposition (ALD) and its applications for electrochemical energy storage and electrocatalysis.

Kuan Hu is currently a post-doctoral researcher in the Department of Advanced Nuclear Medicine Sciences, National Institute of Radiological Sciences, National Institutes for Quantum and Radiological Science and Technology of Japan. He received his PhD degree in Chemical genomics from the School of Chemical Biology and Biotechnology, Peking University Shenzhen Graduate School. Then he moved to Beijing Institute of Nanoenergy and Nanosystems (BINN) of Chinese Academy of Sciences as a research assistant. His research focuses on the synthesis and applications of novel peptide nanomaterials.

Zhe Li received her B.S. degree in the college of science from Northeast Forestry University, Haerbin, China, in 2015. She is currently pursuing her Ph.D. degree in Beijing Institute of Nanoenergy and Nanosystems, Chinese Academy of Sciences. Her research work is focusing on the application of nanogenerator for self-powered biomedical systems, active sensors, and energy storage devices.

Yixiang Jiang received his B. S. in Pharmaceutical Sciences in 2014 from Guangzhou University of Chinese Medicine, China. He then obtained his Ph.D. in Chemical Genomics from the School of Chemical Biology and Biotechnology, Peking University in 2019 under the supervision of Prof. Zigang Li. His research interest mainly focuses on the development and application of novel alpha-helical stabilized peptide, including peptide drugs targeting neurodegenerative disease and peptide self-assembly materials.

Dr. Zigang Li received his B.S. from the University of Science and Technology of China. He obtained his M.S. from Tulane University under the guidance of Professor Chao-Jun Li. Then he moved to the University of Chicago to continue his Ph.D. study under the guidance of Professor Chuan He. He joined Professor Gregory Verdine's group at Harvard University as a postdoctoral fellow in 2009–2010. Then he started his own independent research group at Peking University. His research focuses on developing novel peptide modulators to target various protein/protein interactions and mechanistic study of virulence regulator proteins of infectious pathogens.

Dr. Zhou Li received his Ph.D. from Peking University in Department of Biomedical Engineering in 2010, and bachelor degree from Wuhan University in 2004. He jointed School of Biological Science and Medical Engineering of Beihang University in 2010 as an associate Professor. Currently, he is a Professor in Beijing Institute of Nanoenergy and Nanosystems, CAS. His research interests include nanogenerators, in vivo energy harvester and self-powered medical devices, biosensors.

Dr. Xinwei Wang is currently an Associate Professor at School of Advanced Materials, Shenzhen Graduate School, Peking University, China. He received his Bachelor degree in Physics from Peking University, China, in 2008, and his Ph.D. degree in Chemical Physics from Harvard University in 2012. After a short period of postdoctoral research at Harvard University, he joined the faculty of Peking University in 2013. His research has been mainly focused on thin film materials and their applications for energy and microelectronic devices.